Supporting Information

Cross-species Bio-inspired Anisotropic Surface for Active Droplets Transportation Driven by Unidirectional Microcolumn Waves

Yuegan Song,[†,‡,§] Shaojun Jiang,[†,§] Guoqiang Li,[,‡] Yachao Zhang,[†] Hao Wu,[†] Cheng Xue,[†] Hongshu You,[†] Dehu Zhang,[‡] Yong Cai,[‡] Jiangong Zhu,[‡] Wulin Zhu,[†] Jiawen Li,[†] Yanlei Hu,[*,†] Dong Wu,[†] and Jiaru Chu[†]*

[†] CAS Key Laboratory of Mechanical Behavior and Design of Materials, Key Laboratory of Precision Scientific Instrumentation of Anhui Higher Education Institutes, Department of Precision Machinery and Precision Instrumentation, University of Science and Technology of China, Hefei 230026, China

[‡] School of Manufacturing Science and Engineering, Key Laboratory of Testing Technology for Manufacturing Process, Ministry of Education, Southwest University of Science and Technology, Mianyang 621010, China

[*] Corresponding author: huyl@ustc.edu.cn and guoqli@swust.edu.cn

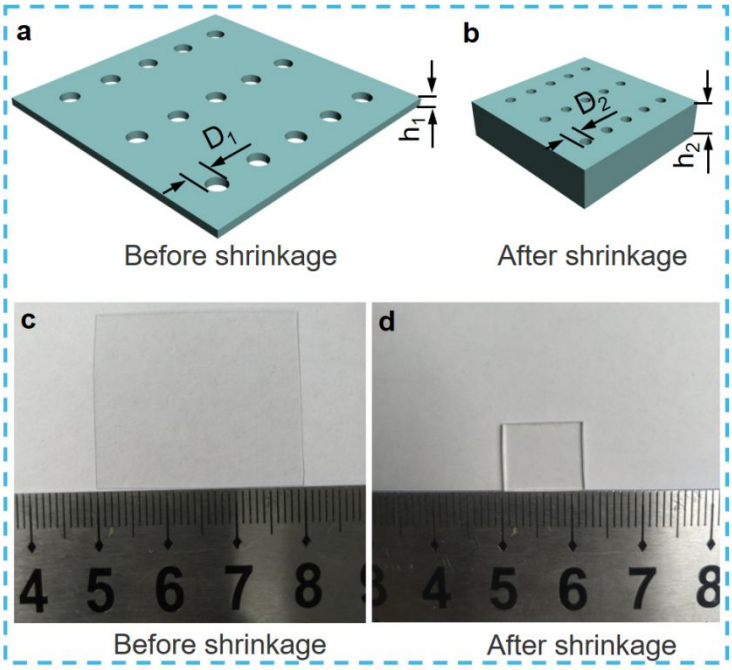

Figure S1. The thermal shrinkage property of shape memory polystyrene (SMP) polymer. The three-dimensional model illustration of SMP polymer a) before and b) after shrinkage. The optical image of SMP sample c) before shrinkage, and d) heated continuously in oven at 130℃ for 10 minutes after shrinkage.

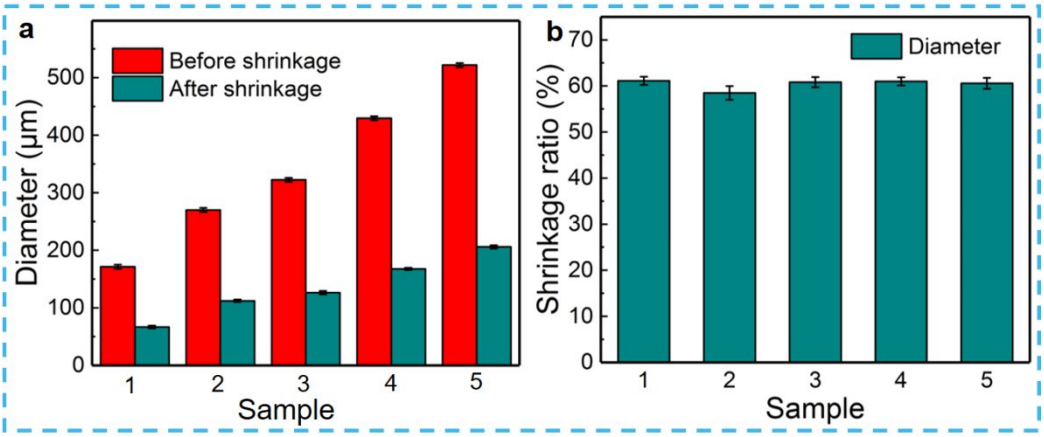

Figure S2. Statistical tables of microholes diameter before and after shrinkage, and shrinkage ratio of five samples. a) Microholes diameter of five samples before and after

shrinkage. b) Shrinkage ratio of five samples after shrinkage.

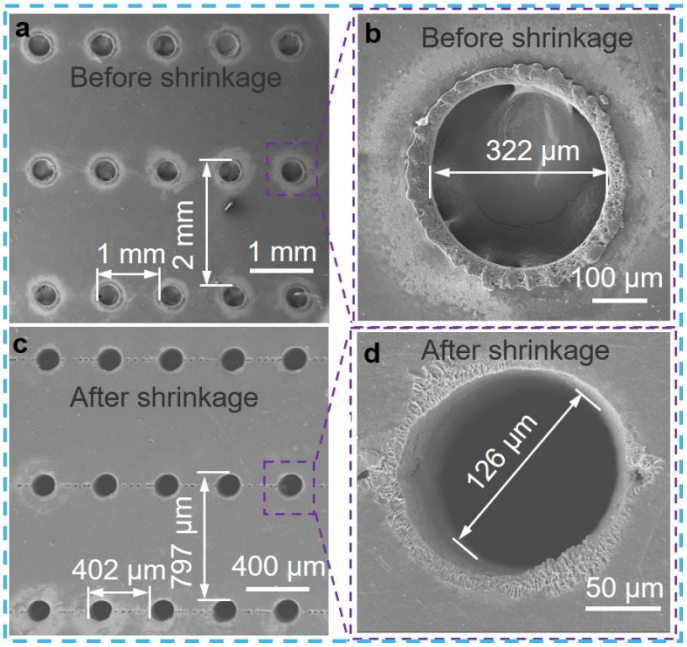

Figure S3. Scanning electron microscopy (SEM) images of microholes array of the third sample before and after shrinkage. SEM images of the third sample microholes array a) before and c) after shrinkage, SEM images of the third sample microhole diameter b) before and d) after shrinkage.

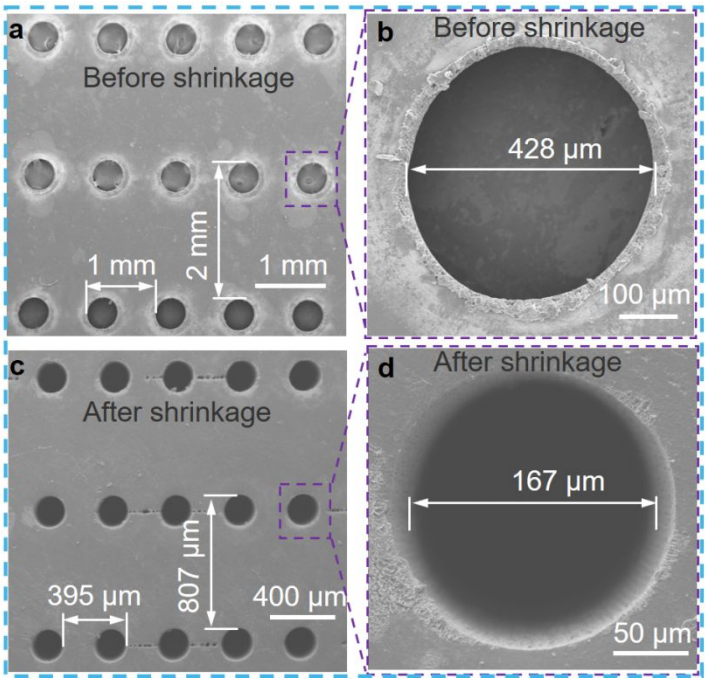

Figure S4. Scanning electron microscopy (SEM) images of microholes array of the fourth sample before and after shrinkage. SEM images of the fourth sample microholes array a) before and c) after shrinkage. SEM images of the fourth sample microhole diameter b) before and d) after shrinkage.

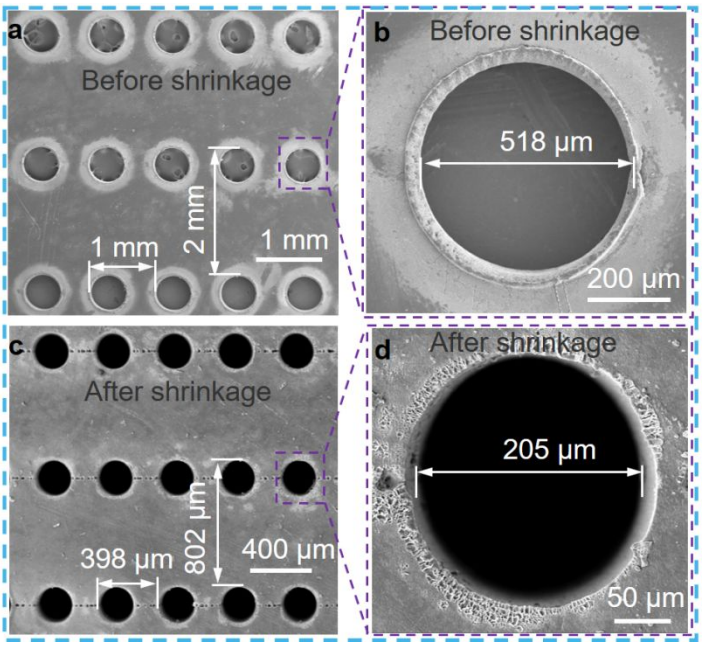

Figure S5. Scanning electron microscopy (SEM) images of microholes array of the fifth sample before and after shrinkage. SEM images of the fifth sample microholes array a) before and c) after shrinkage, SEM images of the fifth sample microhole diameter b) before and d) after shrinkage.

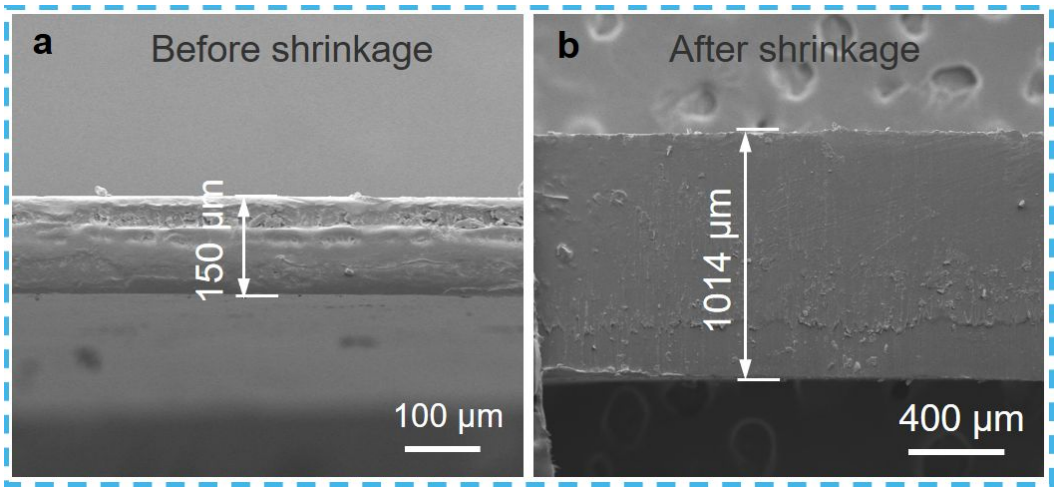

Figure S6. Scanning electron microscopy (SEM) images of the thickness of shape memory polystyrene (SMP) polymer before and after shrinkage. a) SEM image of

SMP before shrinkage, with thickness of ~150 μm. b) SEM image of SMP after shrinkage, with thickness of ~1014 μm.

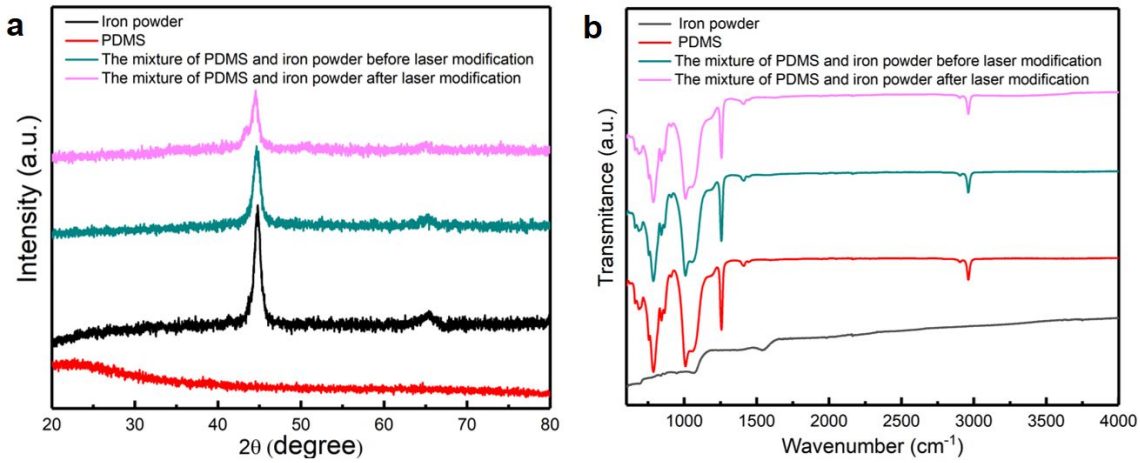

Figure S7. X-ray diffraction (XRD) and Fourier Transform Infrared spectroscopy (FT-IR) characterization of PDMS, iron powder, mixture of PDMS and iron powder before and after laser modification. a) XRD of PDMS, iron powder, mixture of PDMS and iron powder before and after laser modification. b) FT-IR of PDMS, iron powder, mixture of PDMS and iron powder before and after laser modification.

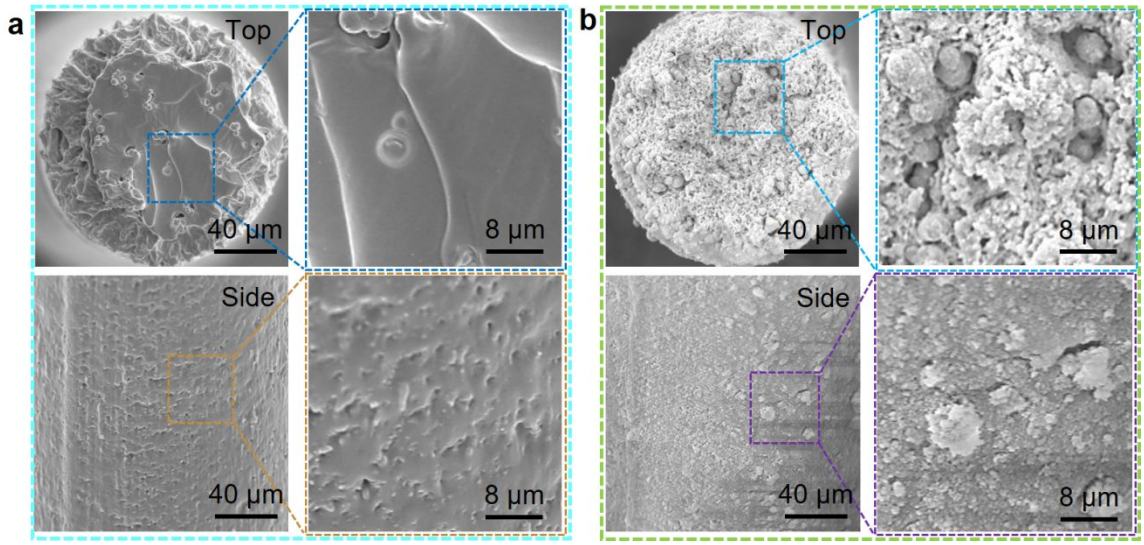

Figure S8. Scanning electron microscopy (SEM) images with high resolution before and after laser modification. a) SEM image with high resolution of the microcolumn before laser modification. b) SEM image with high resolution of the microcolumn after laser modification.

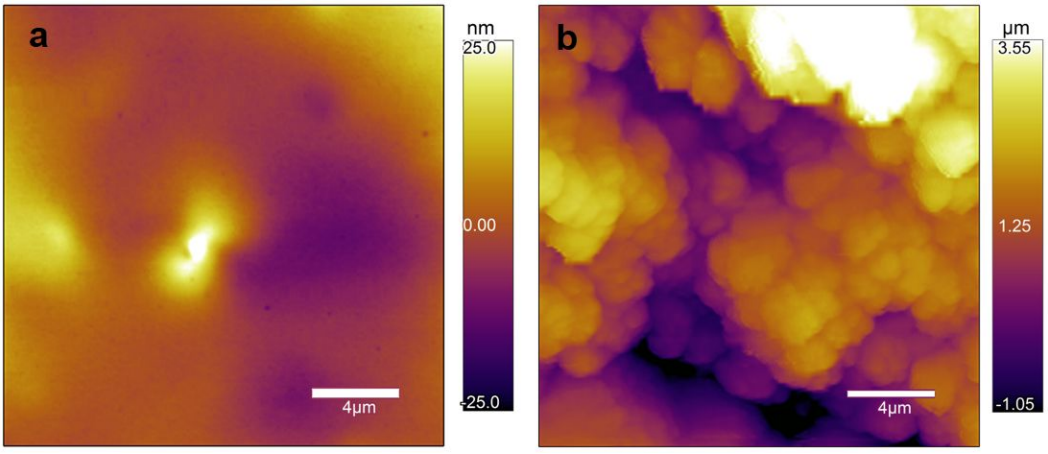

Figure S9. Atomic force microscope (AFM) images of HAR-MRMA surface before and after laser modification. a) AFM image before laser modification with roughness about 6 nm, and b) AFM image after laser modification with roughness about 1.16 μm.

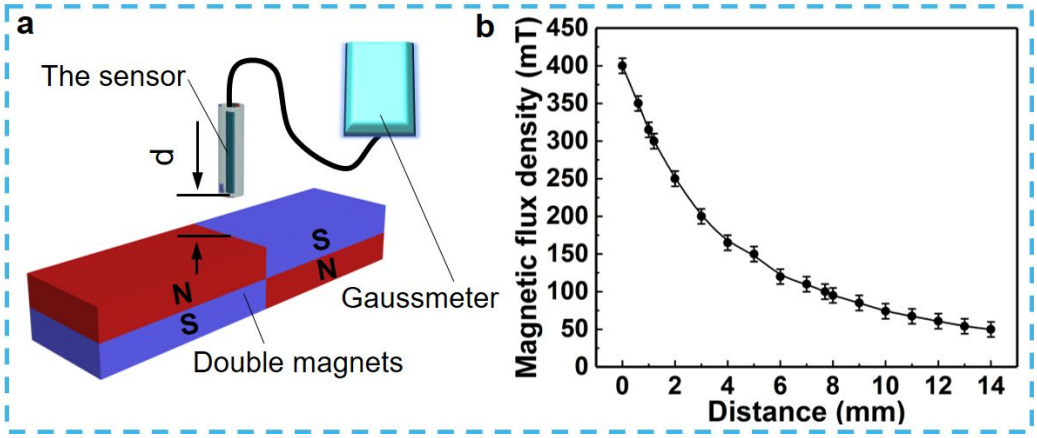

Figure S10. Measurement of the magnetic flux density magnitude. a) Model illustration to measure the magnetic flux density above the two magnets junction. The vertical distance between the sensor connector and magnet is defined as *d*, the magnitude of magnetic flux density is controlled by changing the vertical distance. b) Quantitative relationship between vertical distance *d* and magnetic flux density.

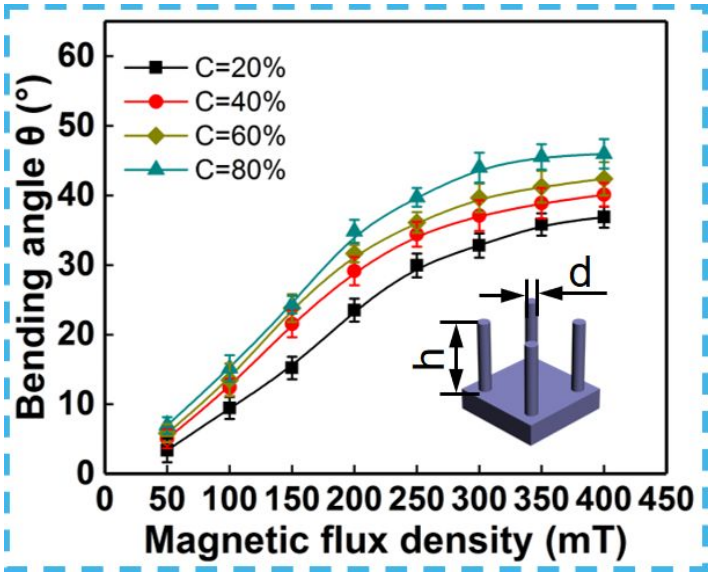

Figure S11. The quantitative relationship between the magnetic flux density and the

bending angle of the microcolumns with the different iron powder concentrations (*C*). C = 20%, C = 40%, C = 60%, and C = 80%, respectively. The diameter of the microcolumns is d = 120 μm. h remains to be 1014 μm.

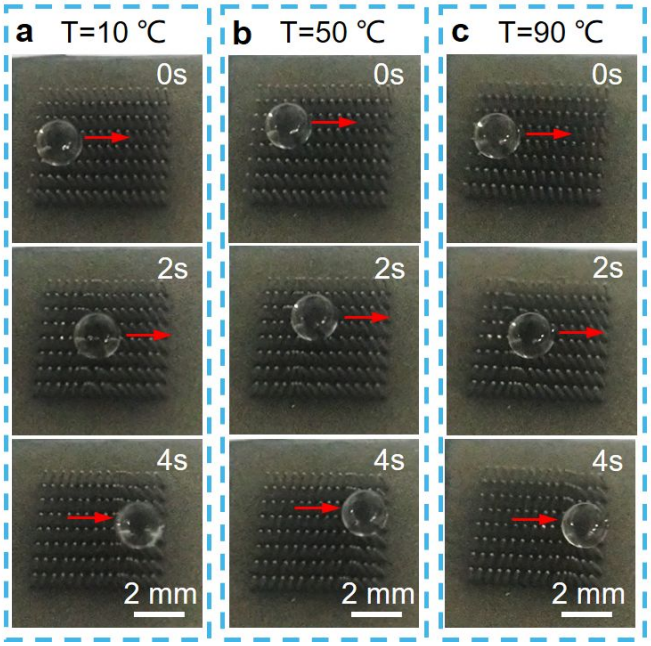

Figure S12. Directional stable transportation of droplet with different temperatures (T). Temperatures of droplet of a) T = 10 ℃, b) T = 50 ℃, c) T = 90 ℃.

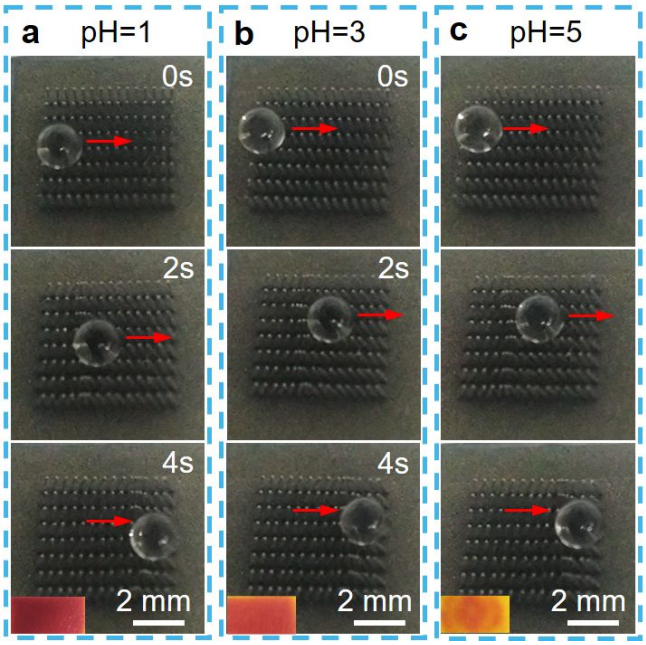

Figure S13. Directional stable transportation of acidic solution (HCI) with different pH. The pH of acidic solution (HCI) is a) pH = 1, b) pH = 3, c) pH = 5, respectively. The illustration in lower left corner shows the pH of the acidic solution (HCI) on a pH strip.

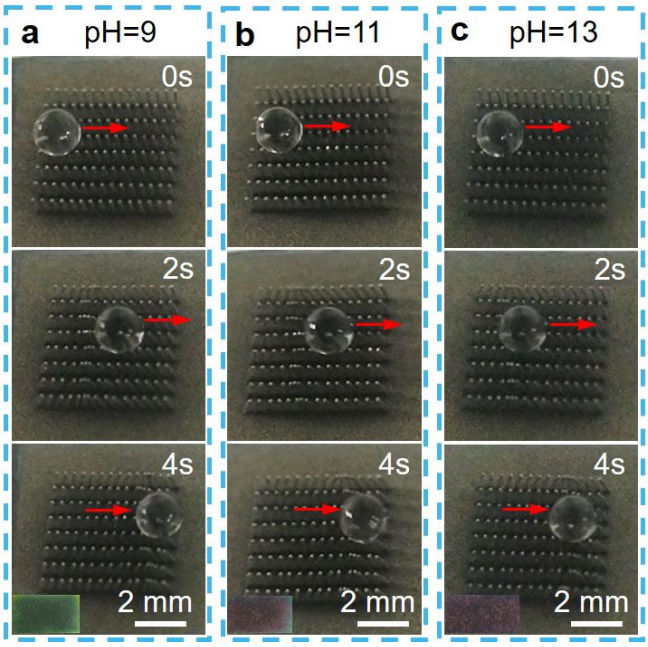

Figure S14. Directional stable transportation of alkaline solution (NaOH) with

different pH. The pH of alkaline solution (NaOH) is a) pH = 9, b) pH = 11, c) pH = 13, respectively. The illustration in lower left corner shows the pH of alkaline solution (NaOH) on a pH strip.